A Solar Radiation Model for Use in Climate Studies

MING-DAH CHOU

Laboratory for Atmospheres, NASA/Goddard Space Flight Center, Greenbelt, Maryland

(Manuscript received 16 May 1991, in final form 3 September 1991)

ABSTRACT

A solar radiation routine has been developed for use in climate studies. It includes the absorption and scattering due to ozone, water vapor, oxygen, carbon dioxide, clouds, and aerosols. Rayleigh scattering is also included. The UV and visible region ($\lambda < 0.69$ μm) is grouped into four bands. An effective coefficient for ozone absorption and an effective cross section for Rayleigh scattering are computed for each band. In the near-infrared region ($\lambda > 0.69$ μm), the broadband parameterization is used to compute the absorption by water vapor in a clear atmosphere, and the k-distribution method is applied to compute fluxes in a scattering atmosphere. The reflectivity and transmissivity of a scattering layer are computed analytically using the delta-four-stream discrete-ordinate approximation. The two-stream adding method is then applied to compute fluxes for a composite of clear and scattering layers. Compared to the results of high spectral resolution and detailed multiple-scattering calculations, fluxes and heating rate are accurately computed to within a few percent.

The high accuracy of flux and heating rate calculations is achieved with a reasonable amount of computing time. With the UV and visible region grouped into four bands, this solar radiation routine is useful not only for climate studies but also for studies on the photolysis in the upper atmosphere and the photosynthesis in the biosphere.

1. Introduction

Solar radiation is the primary source of energy that drives the atmospheric and oceanic circulations. Accurate calculation of solar radiation is therefore important for climate studies. The absorption of solar radiation by ozone, water vapor, oxygen, and carbon dioxide in a nonscattering atmosphere can be accurately computed with a minimal amount of computing time. Simple broadband absorption functions have been developed for water vapor (e.g., Chou 1986; Chou and Arking 1981; Lacis and Hansen 1974), ozone (e.g., Lacis and Hansen 1974), and oxygen and carbon dioxide (e.g., Chou 1990; Kiehl and Yamanouchi 1985; Kiehl et al. 1985). Compared to detailed calculations, errors in the fluxes computed with these broadband models are less than a few watts per square meter. When scattering by atmospheric gases, clouds, and aerosols are involved, calculations of solar fluxes become very complicated and time consuming. Because multiple-scattering algorithms are developed for monochromatic radiative transfer, that is, the transmission function follows Beer's law, the broadband models cannot be applied to computing fluxes in a scattering atmosphere. The spectrum has to be divided or grouped into a large number of regions, which further augments the burden of computations. For climate applications where repeated calculations of radiative transfer are required, it is necessary to simplify the multiple-scattering calculations and optimally group the spectrum into a small number of regions.

In the near-infrared region from 2600 to 14 500 cm^{-1} (0.69–3.85 μm), the spectrum has to be divided into about a half million intervals in order to resolve water vapor absorption lines and to apply Beer's law. The computational burden due to the use of a large number of spectral intervals can be greatly reduced by using the k-distribution method (here k denotes the absorption coefficient). With an appropriate scaling of an inhomogeneous path, Chou (1986) has found that the solar near-infrared fluxes can be accurately computed with a maximum of nine values of k instead of a half million spectral intervals. In the UV and visible region ($\lambda < 0.69$ μm, where λ is the wavelength), the absorption spectrum of ozone is continuous in nature, and it requires fewer spectral intervals than the near-infrared region for accurate computations of solar heating. Nevertheless, it is desirable to reduce the number of spectral intervals, yet still maintain a high degree of accuracy in solar heating computations, because the amount of computing time is proportional to the number of intervals used.

In climate studies, computations of solar fluxes in a multiple-scattering atmosphere are usually highly simplified with large errors. Recently, a numerically stable discrete-ordinate algorithm was developed by Stamnes et al. (1988). This algorithm is applicable to a multiple-scattering, vertically inhomogeneous plane-parallel at-

Corresponding author address: Dr. Ming-Dah Chou, NASA/Goddard Space Flight Center, Climate and Radiation Branch Laboratory for Atmospheres, Code 913, Greenbelt, MD 20771.

mosphere. The accuracy of flux calculations depends on the number of discrete-ordinate streams used. High-accuracy flux calculations can be achieved by using only four streams. This algorithm is comprehensive but time consuming, especially when the number of atmospheric layers is large. For a numerical climate model where repeated calculations are required, a much faster algorithm is highly desirable. Because of its accuracy and versatility, however, this algorithm can be used to compute fluxes for validating results from a simplified model.

In this study, an efficient algorithm is developed for computing solar fluxes due to the absorption by ozone and water vapor, and the absorption and scattering by clouds, aerosols, and atmospheric gases. Three major steps are taken in the algorithm development: 1) optimal grouping of spectral regions; 2) computation of absorption and scattering properties in individual spectral groups; and 3) simplification of the multiple-scattering algorithm. Fluxes and heating rate computed with this algorithm are validated against the results of high spectral-resolution calculations using the algorithm of Stamnes et al. (1988).

2. Atmospheric, cloud, and aerosol models

The absorption of solar radiation by ozone and water vapor is computed for a midlatitude summer atmosphere as defined in McClatchey et al. (1972). The atmosphere is divided into 42 layers. Below the 100-mb level, there are 20 layers with $\Delta p = 50$ mb, where p is the pressure. Above the 100-mb level, the interval of each layer is $\Delta \ln p = 0.34$. From the values given in McClatchey et al. (1972), temperature, ozone, and the logarithm of humidity of each layer are interpolated linearly with the logarithm of pressure.

A cirrus cloud and a stratus cloud are used for computing solar fluxes. The cirrus cloud is set in the 225–275-mb layer, and the stratus cloud is in 800–900 mb. Taken from the values specified in the intercomparison of Radiation Codes in Climate Models (ICRCCM) (Ellingson and Fouquart 1990), the cloud-scattering optical thickness is assumed to be independent of wavelength and is set to 2.8 for the cirrus cloud and 9.7 for the stratus cloud. The cloud single-scattering albedo is set to 1 in the UV and visible region and is taken from the values given by King et al. (1990) for individual water vapor absorption bands in the near-infrared region. Because the absorption spectra due to water vapor and cloud droplets follow each other closely, the cloud absorption of solar radiation near the centers of the absorption bands is strong. It follows that flux calculations near the band centers are not sensitive to the single-scattering albedo. Therefore, the single-scattering albedos representative of the regions between absorption bands are used for computing the absorption by clouds. Values of the single-scattering albedo used in this study are listed in Table 1 for the seven water vapor absorption bands. It should be noted that our knowledge on the absorption of solar radiation within clouds is rather limited. It has been well acknowledged that the cloud absorption derived from aircraft measurements is significantly higher than the theoretical calculations. Stephens and Tsay (1990) reviewed the theories of cloud darkening and concluded that no one theory can definitively explain the discrepancies between theory and measurement of solar radiative transfer in clouds. The uncertainty in the cloud single-scattering albedo used here might be large. Nevertheless, it is not a subject of this study. The cloud asymmetry factor is set to 0.843 for all wavelengths for both the cirrus and the stratus clouds. This cloud asymmetry factor is computed from Mie theory for the stratus water droplets. Although the asymmetry factor for the cirrus ice crystals is expected to be different from this value, the use of the same asymmetry factor for both clouds should not affect the conclusion of this study.

TABLE 1. The spectral range of water vapor absorption bands and the cloud single-scattering albedo.

Band (μm)	Spectral range (cm^{-1})	Cloud single-scattering albedo
0.72	13120–14500	0.999
0.82	11600–13120	0.999
0.94	9600–11600	0.995
1.14	8200–9600	0.990
1.38	6320–8200	0.980
1.87	4400–6320	0.970
2.7/3.2	2600–4400	0.960

The Maritime I aerosol model given in the ICRCCM is adopted in this study. The aerosol is distributed between the 225-mb level and the surface. The aerosol optical thickness is set to 0.025 in the region from 225 mb to 800 mb and 0.05 below the 800-mb level. It is assumed to be distributed evenly with mass within these two regions. Also taken from the values given in the ICRCCM, the aerosol asymmetry factor and the single-scattering albedo are set, respectively, to 0.636 and 0.891 above the 800-mb level and 0.743 and 0.989 below.

3. Detailed calculations

Ozone absorbs solar radiation in the UV and visible region ($\lambda < 0.69$ μm) and is the dominant contributor in heating the middle atmosphere (0.01–40 mb). Although the absorption coefficient of ozone is rather smooth with wavelength, it ranges by more than five orders of magnitude. Therefore, it is necessary to divide the spectrum into a large number of small intervals for accurate flux calculations. On the other hand, the water vapor contributes significantly to the heating of the lower troposphere. Water vapor has a rich absorption spectrum that fluctuates strongly within very narrow

spectral intervals. Line-by-line methods are required for achieving a high degree of accuracy in flux calculations.

The spectrum between 0.175 μm and 0.69 μm is divided into 127 intervals with a resolution of 1.5–5 nm. The cross sections for ozone absorption and the Rayleigh scattering, as well as solar flux, are taken from a World Meteorological Organization report on atmospheric ozone (World Meteorological Organization 1985) and are plotted in Fig. 1. Pressure has no effect on the ozone absorption, while temperature has a noticeable effect only in the region from 0.28 μm to 0.35 μm. In this study, the ozone absorption coefficient in this spectral region is fixed at the values corresponding to the absorption at 225 K. In the near-infrared region between 0.69 μm and 3.85 μm, the spectrum is divided into a half million intervals with a resolution of 0.025 cm^{-1}. Chou (1986) has found that this spectral resolution is adequate for accurate computations of the near-infrared fluxes. The water vapor absorption coefficient as a function of wavenumber, pressure, and temperature is computed monochromatically using the line-by-line method of Chou and Kouvaris (1986). The 1982 version of the Air Force Geophysical Laboratory molecular line parameters (Rothman et al. 1983) is used to compute the coefficient for each absorption line.

When there are more than one absorber and scatterer in an atmospheric layer, the effective optical parameters required for flux computations are approximated by (cf. Tsay et al. 1989)

$$\tau = \sum \tau_i, \tag{1a}$$

$$\omega = \sum \omega_i \tau_i / \sum \tau_i, \tag{1b}$$

and

$$g^l = \sum (g^l \omega_i \tau_i) / \sum (\omega_i \tau_i). \tag{1c}$$

Here τ, ω, and g denote, respectively, the optical thickness, single-scattering albedo, and asymmetry factor, and i is the index for gases and particulates. The summation is over gases and particulates. The exponent l goes from 1 to n, where $n - 1$ is the number of streams used. The scattering phase matrix is assumed to follow the Henyey–Greenstein function.

The high-resolution spectral data of scattering and absorption are incorporated into the algorithm of Stamnes et al. (1988) to accurately compute solar fluxes in both scattering and nonscattering atmospheres. The accuracy of the algorithm varies with the number of the discrete-ordinate streams used. High spectral resolution calculations of the fluxes in the water vapor band from 8200 to 9600 cm^{-1} show that the difference between the use of four streams and eight streams is <0.4% at all heights. However, the computing time required for the use of four streams is an order of magnitude smaller than that required for the use of eight streams. Therefore, a number of 4 for the discrete-ordinate streams is used in this study. Results of the detailed flux calculations serve as benchmarks for validating the parameterizations.

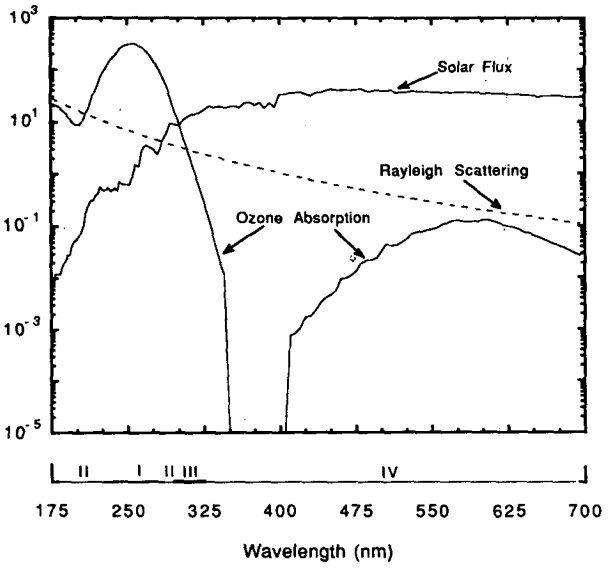

FIG. 1. The spectral distributions of the solar flux and of the cross sections of Rayleigh scattering and ozone absorption in the UV and visible region. Only relative magnitudes are shown; units are arbitrary. The spectral ranges of the four bands are shown at the bottom of the figure.

4. Simplification of multiple-scattering calculations

In climate studies, radiative transfer calculations require an efficient routine for taking into account the multiple scattering by atmospheric gases, clouds, and aerosols. Liou et al. (1988) developed an analytic solution for the delta-four-stream approximation for computing reflectance and transmittance of atmospheric layers. Compared to the "exact" results of the adding–doubling method, the relative errors in transmission, absorption, and reflection are generally within 5% for the entire ranges of the solar zenith angle and the single-scattering albedo and for the range of the optical thickness of 0.1–50.

The analytical solution for the delta-four-stream approximation is computationally fast but can only be applied to individual layers. In this study, the algorithm of Liou et al. (1988) for layer transmittance and reflectance is combined with the two-stream adding method to compute the transmittance and reflectance for a composite of layers. For each scattering layer, transmittance and reflectance illuminated by beam radiation (T and R) and by diffuse radiation (T^* and R^*) are computed from Liou's routine. Detailed calculations of T^* and R^* are time consuming, because they require integration over angles. To simplify the calculations, it is assumed that the transmittance and

reflectance of diffuse radiation can be approximated by that of beam radiation with an incident angle of 53°. For each nonscattering layer, transmittances and reflectances are given by

$$T = \exp(-kw/\mu_0) \tag{2a}$$

$$T^* = \exp(-1.66kw). \tag{2b}$$

$$R = R^* = 0 \tag{2c}$$

where k is the absorption coefficient, w is the absorber amount, μ_0 is the cosine of the solar zenith angle, and the constant 1.66 ($=1/\cos 53°$) is the diffusivity factor commonly used for approximating the diffuse transmittance. The surface is considered as one layer with $T = T^* = 0$.

The reflectance of a combination of the layer a and the layer below, b, when illuminated by diffuse radiation from above, R^*_{ab}, is generally different from that when illuminated from below, R^{**}_{ab}. They are computed from

$$R^*_{ab} = R^*_a + T^*_a R^*_b T^*_a/(1 - R^{**}_a R^*_b), \tag{3a}$$

$$R^{**}_{ab} = R^*_b + T^*_b R^{**}_a T^*_b/(1 - R^{**}_a R^*_b), \tag{3b}$$

where the superscripts * and ** denote illumination from above and below, respectively. The diffuse transmittances of a combination of layers a and b are computed from

$$T^*_{ab} = T^{**}_{ab} = T^*_a T^*_b/(1 - R^{**}_a R^*_b). \tag{3c}$$

By separating the direct and diffuse components of the radiation, the reflectance and transmittance of a combination of two layers when illuminated by beam radiation are computed from (cf. Coakley et al. 1983)

$$R_{ab}(\mu_0) = R_a(\mu_0) + T^*_a\{\exp(-\tau_a/\mu_0)R_b(\mu_0) + [T_a(\mu_0) - \exp(-\tau_a/\mu_0)]R^*_b\}/(1 - R^{**}_a R^*_b), \tag{4a}$$

$$T_{ab}(\mu_0) = \exp(-\tau_a/\mu_0)T_b(\mu_0) + T^*_b\{\exp(-\tau_a/\mu_0)R^{**}_a R_b(\mu_0) + [T_a(\mu_0) - \exp(-\tau_a/\mu_0)]\}/(1 - R^{**}_a R^*_b), \tag{4b}$$

where $T(\mu_0)$, $\exp(-\tau/\mu_0)$, and $[T(\mu_0) - \exp(-\tau/\mu_0)]$ are the total, direct, and diffuse transmittances, respectively. The reflection, $F\uparrow$, and transmission, $F\downarrow$, of solar flux at the level $i + 1/2$ (the lower boundary of the layer i) are then derived from

$$F\uparrow = \{\exp(-\tau_{1,i}/\mu_0)R_{i+1,k}(\mu_0) + [T_{1,i}(\mu_0) - \exp(-\tau_{1,i}/\mu_0)]R^*_{i+1,k}\}/(1 - R^{**}_{1,i} R^*_{i+1,k}), \tag{5a}$$

$$F\downarrow = \exp(\tau_{1,i}/\mu_0) + \{\exp(-\tau_{1,i}/\mu_0)R^{**}_{1,i} R_{i+1,k}(\mu_0) + [T_{1,i}(\mu_0) - \exp(-\tau_{1,i}/\mu_0)]\}/(1 - R^{**}_{1,i} R^*_{i+1,k}), \tag{5b}$$

where the index k denotes the surface and the subscripts $(1, i)$ and $(i + 1, k)$ denote the regions above and below the level $i + 1/2$, respectively. The transmittance, $T_{1,i}$, and reflectance, $R^{**}_{1,i}$, of the region above the level $i + 1/2$ are computed by adding layers from the top of the atmosphere down to the surface according to the procedures given in Lacis and Hansen (1974). On the other hand, the reflectances, $R_{i+1,k}$ and $R^*_{i+1,k}$, are computed by adding layers from the surface up to the top of the atmosphere.

5. Ultraviolet and visible region

Solar radiation in the ultraviolet and visible regions is important not only to climate but also to photolysis in the upper atmosphere and to photosynthesis for plants on land and in the oceans. The parameterization of ozone absorption by Lacis and Hansen (1974), which treats the entire UV and visible region as one band, is simple and accurate. Using the high-resolution spectral data given in World Meteorological Organization (1985), I have computed the flux-weighted absorptance for the entire UV and visible region. It is found that the difference between the high-resolution calculations and the Lacis and Hansen parameterization is within a few percent. For application to a scattering atmosphere, however, calculations have to be reduced to a case equivalent to monochromatic so that Beer's law and, hence, multiple-scattering algorithms can be applied. Furthermore, it is desirable to separate the ultraviolet radiation from the photosynthetically active radiation (PAR) for the photolysis and biology studies.

In a study on the atmospheric heating and photodissociation, Stamnes and Tsay (1990) divided the UV and visible region (0.175–0.7 μm) into four bands. The effective absorption coefficient for each band is derived by weighting the spectral absorption coefficient with solar flux,

$$k = \int k_\lambda S_\lambda d_\lambda \Big/ \int S_\lambda d_\lambda, \tag{6}$$

where k is the absorption coefficient, S is the incoming solar flux at the top of the atmosphere, and λ is the wavelength. They found that the error in the heating rate computed with the effective absorption coefficient is <20%. In the present study, the accuracy of flux and heating rate calculations is further enhanced by taking the following two measures: 1) grouping spectral re-

gions with similar absorption properties and 2) deriving the effective absorption coefficient using regression instead of using (6).

It can be seen in Fig. 1 that the region from 0.35 to 0.4 μm is free of ozone absorption. In the broad Chappuis band from 0.4 to 0.69 μm, the absorption is weak and the range of the coefficient is relatively narrow. At the higher-wavelength tail of the Huggins band (0.325–0.35 μm), the ozone absorption is weak. In these spectral regions, transmission is rather linear with the absorption coefficient because of weak absorption. They are grouped into one broad band in this study. In the Hartley and Huggins bands with $\lambda < 0.325$ μm, the absorption coefficient does not vary monotonically with wavelength. Furthermore, it varies by more than six orders of magnitude. This spectral region is divided into two contiguous bands (0.225–0.285 μm and 0.3–0.325 μm) and one noncontiguous band (0.175–0.225 μm; 0.285–0.3 μm). The grouping of noncontiguous spectral regions reduces the number of bands and enhances the accuracy of flux calculations. Thus, the UV and visible region is grouped into four bands in this study, the same number of bands as in Stamnes and Tsay (1990).

For each of the four bands, band transmittances are computed as a function of the ozone amount, w, from

$$\tau(w) = \int S_\lambda \exp(-k_\lambda w) d\lambda \Big/ \int S_\lambda d\lambda. \quad (7)$$

The high spectral-resolution data of S_λ and k_λ given in World Meteorological Organization (1985) are used in the computation of $\tau(w)$. The band transmittances are then fit by the function

$$\tau_{app}(w) = \exp(-k_{eff} w), \quad (8)$$

so that the square of the difference between $\tau(w)$ and $\tau_{app}(w)$ is minimized, where k_{eff} is the regression coefficient representing the effective absorption coefficient of the band. Values of k_{eff} are given in Table 2. Figure 2 shows the two transmittances, $\tau(w)$ (solid curves) and $\tau_{app}(w)$ (pluses, "+"), for the four bands. It can be seen in the figure that the band transmittance can be fit well with Beer's function, especially for band 4,

TABLE 2. The spectral range, integrated solar flux, effective ozone absorption coefficient, and effective Rayleigh scattering optical thickness for the four bands in the UV and visible region.

Band	Spectral range (nm)	Solar flux (W m^{-2})	Ozone absorption coefficient [(cm-atm)$^{-1}_{STP}$]	Rayleigh scattering optical thickness (mb^{-1})
1	225–285	7.25	175.30	0.00188
2	175–225 285–300	6.90	26.70	0.00158
3	300–325	15.16	1.99	0.00095
4	325–690	600.92	0.05	0.00017

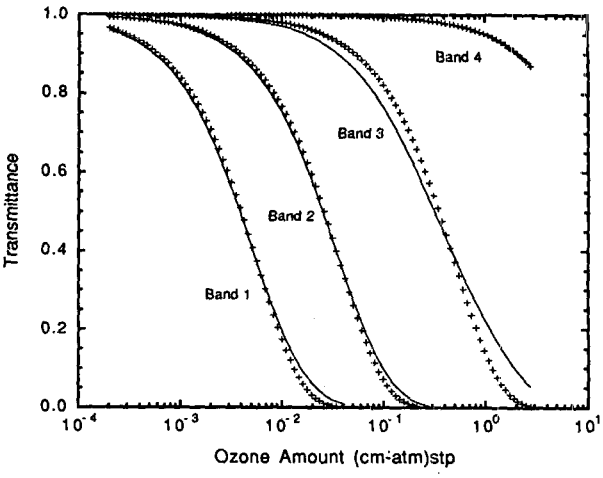

FIG. 2. Band transmittances in the four spectral regions defined in Table 2. The solid curves are detailed calculations using (7), and the dashed curves are regressions using (8).

where absorption is weak and the transmission function is rather linear with the optical thickness, $k_\lambda w$. Apparently, the wide spectral range of this band does not affect the accuracy of the regression.

It is important to understand the effect of grouping spectral regions on the computations of solar heating due to ozone. In the study of Stamnes and Tsay (1990), the spectrum from 0.175 μm to 0.29 μm is treated as one band, and the effective absorption coefficient is computed from (6). The use of (6) for deriving the band absorption coefficient is correct only if absorption is very weak. Otherwise, the absorption will always be overestimated. Figure 3 shows the transmittances in the 0.175–0.3-μm band derived from detailed spectral integrations (solid curve) and from the use of (6) (dashed curve). It can be seen that the averaging procedure of (6) systematically underestimates the transmittance except for a very small amount of ozone. The least-square fit to the band transmittances using Beer's function is also shown in Fig. 3 (pluses, "+"). The difference with the detailed spectral integration remains large. These results indicate that when the magnitude and range of the absorption coefficient in a spectral band are both large, the transmittance cannot be correctly represented by Beer's function. By comparing these results with that of bands 1 and 2, shown in Fig. 2, it is quite impressive to see that the accuracy in transmittance computations is greatly improved by simply grouping the 0.175–0.3-μm region into two.

In grouping the spectral regions, considerations must also be given to the absorbers and scatterers other than ozone. For the Rayleigh scattering, the cross section varies slowly ($\sim\lambda^{-4}$) as opposed to the rapid change of the ozone absorption coefficient. The effective scattering cross section is computed in a similar way as the ozone absorption coefficient. The band from 0.325 μm to 0.69 μm is wide, and the scattering cross section

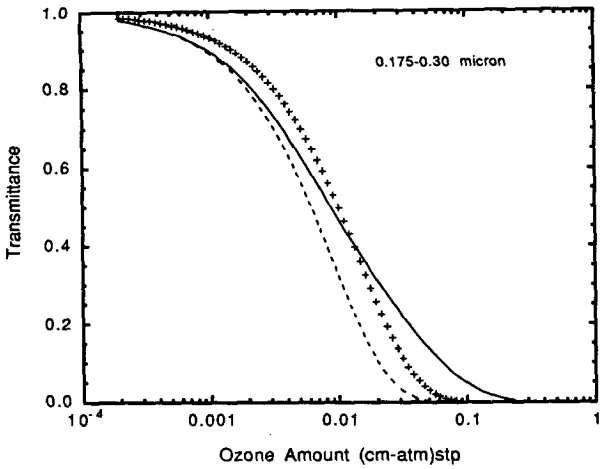

FIG. 3. Band transmittances in the spectral region 0.175–0.30 μm. The solid curve is derived using the detailed calculation of (7), the dashed curve is computed with an absorption coefficient derived from (6), and the pluses ("+") are computed with an absorption coefficient derived from least-squares fit to the detailed calculations.

ranges by a factor of 20. However, the band transmittance for the direct component of the radiation can be fit well by Beer's function because of a small Rayleigh cross section. For the other three bands, the cross section is about an order of magnitude larger, but the spectral intervals are narrower. Therefore, the direct band transmittance can still be fit well by Beer's function. The effective optical thicknesses for the Rayleigh scattering are given in Table 2 for the four bands.

Table 3 shows the net downward fluxes in the 0.175–0.69-μm region at the top of the atmosphere and at the surface of the midlatitude summer atmosphere using the detailed calculations and the parameterization. Two solar zenith angles, 30° and 60°, are used. Absorption by ozone and aerosols and scattering by atmospheric gases, clouds, and aerosols are included. For the detailed calculations, the high spectral resolution (127 bands) of the ozone absorption coefficient and the Rayleigh scattering cross section shown in Fig. 1 as well as the algorithm of Stamnes et al. (1988) are used. For the parameterization, the UV and visible region is grouped into four bands, and reflectances and transmittances are computed using the routine of Liou et al. (1988) and the two-stream adding method.

The top two groups of the calculations shown in the table are for clear situations without clouds and aerosols. Only ozone absorption and Rayleigh scattering are included. The difference in fluxes between the detailed calculations and parameterization is negligible, <0.8 W m^{-2}, both at the top of the atmosphere and at the surface. It can be seen that ozone absorbs 32 and 24 W m^{-2} of solar radiation for $\theta_0 = 30°$ and 60°, respectively. The effect of Rayleigh scattering on the atmospheric absorption is very small, 1 W m^{-2}. It can also be seen from the table that the effect of the Rayleigh scattering on the absorption of solar radiation at the surface is significant. Due to the Rayleigh scattering, the solar radiation absorbed at the surface is reduced by 29 W m^{-2} and 31 W m^{-2}, respectively, for $\theta_0 = 30°$ and 60°. This effect is comparable to that of the absorption due to ozone.

The changes in the atmospheric absorption and in the downward surface fluxes induced by Rayleigh scattering are shown in Table 4 (the top group in the table). The results of the parameterization are very close to that of the high-resolution calculations (labeled HR+DISORT4). The median values as derived from Table 5 of the ICRCCM report are also shown in the table. Compared to the high-resolution, detailed calculations, the ICRCCM median value of the change in the downward surface flux is larger by 6 W m^{-2}, indicating a larger Rayleigh scattering. The ICRCCM report does not provide information on the effect of the absorption by ozone alone. Comparison for the ozone absorption is not given in the table.

When aerosols and clouds are present, the difference between the fluxes of detailed calculations and parameterization increases. Table 3 shows that the difference is <2.5 W m^{-2} for the cirrus case and <7.5 W m^{-2} for the stratus case. The thickness of the cirrus cloud is set to 50 mb, which is the thickness of a tropospheric layer. The reflectance and transmittance of the cloud are properly computed using the four-stream discrete-ordinate algorithm. On the other hand, the thickness of

TABLE 3. The net downward solar fluxes at the top of the atmosphere and at the surface in the 0.175–0.69-μm spectral region for a midlatitude summer atmosphere. The Maritime I aerosols defined in the ICRCCM are used. The surface albedo is set to 0.2. θ_0 is the solar zenith angle. The units of fluxes are watts per square meter.

	Top		Surface	
	$\theta_0 = 30°$	$\theta_0 = 60°$	$\theta_0 = 30°$	$\theta_0 = 60°$
Ozone				
127 bands; DISORT4	450.7	261.0	418.4	237.4
4 bands; ADD	450.8	261.1	418.7	237.3
Ozone + Rayleigh scattering				
127 bands; DISORT4	422.5	230.6	389.4	206.6
4 bands; ADD	423.3	230.6	389.8	206.1
Ozone + Rayleigh scattering + aerosols + cirrus cloud				
127 bands; DISORT4	371.4	173.7	331.3	144.7
4 bands; ADD	369.1	171.5	330.8	144.4
Ozone + Rayleigh scattering + aerosols + stratus cloud				
127 bands; DISORT4	272.7	129.7	224.5	95.4
4 bands; ADD	269.5	122.2	223.8	90.0

Note: DISORT4 denotes the discrete-ordinate algorithm (with 4 streams) of Stamnes et al. (1988), and ADD denotes the two-stream adding method.

TABLE 4. Changes in the atmospheric absorption and in the downward surface fluxes induced by Rayleigh scattering, water vapor, and stratus cloud. A midlatitude summer atmosphere is used for the calculations. The surface albedo and the solar zenith angle are set to 0.2 and 30°, respectively. The units of fluxes are W m^{-2}. Comparison for the stratus cloud case is not consistent. See the text for more detail.

	Atmosphere	Surface
Rayleigh scattering		
HR + DISORT4	0.8	−36.3
Parameterization	1.4	−36.1
ICRCCM (case 31)	1.3	−42.3
Water vapor		
LBL	170.7	−162.3
Parameterization	172.2	−163.7
ICRCCM (case 1)	168.2	−159.9
Stratus cloud[a]		
LBL + DISORT4	104.6	−463.8
Parameterization	101.6	−473.9
ICRCCM (case 49)	55.6	−412.3

[a] The CL cloud defined in the ICRCCM. The cloud optical thickness at 0.55 μm is set to 9.7, and the cloud top is set at 2 km above the surface.

HR: High spectral resolution with 127 intervals in the UV and visible region.
DISORT4: The discrete-ordinate algorithm (with 4 streams) of Stamnes et al. (1988).
Parameterization: The parameterization of this study.
ICRCCM: The median value from the Intercomparison of Radiation Codes in Climate Models (Ellingson and Fouquart 1988).
LBL: Line-by-line calculations.

TABLE 5. The net downward near-infrared (2600–14 500 cm^{-1}) fluxes for a midlatitude summer atmosphere. LBL denotes the line-by-line calculations, and DISORT4 denotes the algorithm of Stamnes et al. (1988). For the parameterization, the *k*-distribution method for water vapor absorption and the two-stream adding method for multiple scattering are used. The surface albedo is set to 0.2. θ_0 is the solar zenith angle. The units of fluxes are watts per square meter.

Absorption band	Top		Surface	
	$\theta_0 = 30°$	$\theta_0 = 60°$	$\theta_0 = 30°$	$\theta_0 = 60°$
H_2O only				
LBL + DISORT4	546.1	316.8	375.4	206.0
Broadband, Eq. (11)	546.5	316.8	374.3	205.2
H_2O + aerosol + cirrus cloud				
LBL + DISORT4	479.9	224.1	298.5	129.0
Parameterization	479.2	224.1	294.3	129.5
H_2O + aerosol + stratus cloud				
LBL + DISORT4	429.9	217.8	167.2	69.7
Parameterization	421.9	214.5	158.7	66.1

the stratus cloud is set to 100 mb, which spans two tropospheric layers. Errors are introduced in the cloud reflectance and transmittance due to the use of the two-stream adding approximation. This is the main reason for a larger error in the stratus case than in the cirrus case.

Figure 4 shows the solar heating profiles for the midlatitude summer atmosphere. The calculation includes the absorption due to ozone and aerosols and the scattering due to gases, aerosols, and clouds. The heating rate profile of the parameterization (dashed curve) is close to that of the detailed calculations (solid curve) with a difference of <1.0°C day^{-1}, which is 5% of the peak heating rate. Except for a narrow region in the atmosphere, the heating due to ozone is underestimated.

6. Near-infrared region

Absorption and scattering of solar radiation in the near-infrared from 0.69 μm to 3.85 μm (2600–14 500 cm^{-1}) are primarily due to water vapor, clouds, and aerosols. In a nonscattering atmosphere, the solar flux, $F(p)$, reaching the pressure level p can be computed from

$$F(p) = \mu_0 \int S_\lambda \tau_\lambda(p) d\lambda, \qquad (9)$$

where the function $\tau_\lambda(p)$ is the transmittance between

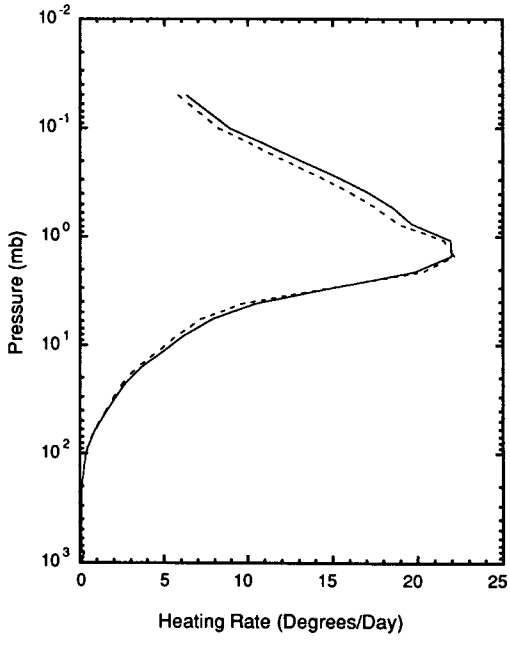

FIG. 4. Heating rate profiles in the UV and visible region for a midlatitude summer atmosphere with a solar zenith angle of 30°. The calculations include absorption and scattering due to ozone, aerosols, a stratus cloud, and atmospheric gases. The solid curve is the detailed calculation, and the dashed curve is the parameterization.

the top of the atmosphere and the level p. The broadband transmission function is then defined as

$$\tau(p) = \int S_\lambda \tau_\lambda(p) d\lambda \Big/ \int S_\lambda d\lambda. \quad (10)$$

The half-width of an absorption line in the troposphere is in the range 0.01–0.1 cm^{-1}, and the absorption coefficient varies rapidly with wavenumber. Detailed calculations of the near-infrared flux using (9) requires an integration of fluxes at about half a million spectral intervals. Chou (1986) found that calculations of the near-infrared fluxes can be greatly simplified, yet can still maintain a high degree of accuracy by using the following scaling approximation:

$$w = w'(p/p_r)^{0.8} \exp[0.00135(T - T_r)], \quad (11)$$

where w is the scaled water vapor amount, w' is the water vapor amount, p_r = 300 mb, and T_r = 240 K.

With use of the scaling approximation, the broadband transmission function becomes a function only of the scaled water vapor amount. Chou (1986) computed the broadband transmission function at 300 mb and 240 K for the entire near-infrared region using the line-by-line method, and fit the transmission function by

$$\tau(w) = \exp[-11.5w/(1 + 10.5w + 64w^{0.59})]. \quad (12)$$

The solar flux at the pressure level p can then be easily computed from

$$F(p) = 0.5343\mu_0 S_0 \tau[w(p)/\mu_0]. \quad (13)$$

Here w is the scaled water vapor amount above the level p and S_0 is the solar constant. The constant, 0.5343, is the fraction of solar energy contained in the spectral region 2600–14 500 cm^{-1}.

For a clear atmosphere where only water vapor is concerned, absorption of solar radiation is easily computed from (11)–(13). The net downward fluxes at the top of the atmosphere and at the surface of the clear midlatitude summer atmosphere are shown in the top group of Table 5. Two solar zenith angles, θ_0 = 30° and 60°, are used in the calculations. For the detailed calculations, the water vapor absorption coefficient is computed as a function of layer pressure and temperature at 0.025 cm^{-1} spectral intervals using the line-by-line method. The algorithm of Stamnes et al. (1988) is used to accurately compute the absorption of solar radiation reflected by the surface. It can be seen in the table that the parameterization introduces very small errors in the fluxes. The error is $\approx$1 W m^{-2} at the surface and is negligible at the top of the atmosphere. Figure 5 shows the heating rate profiles for the detailed calculations (solid curves) and the parameterization using (12) (dashed curves). Except in the upper stratosphere, the error in the parameterization is <0.1°C day^{-1}. The large error (0.3°C day^{-1}) in the upper stratosphere is caused by the pressure scaling

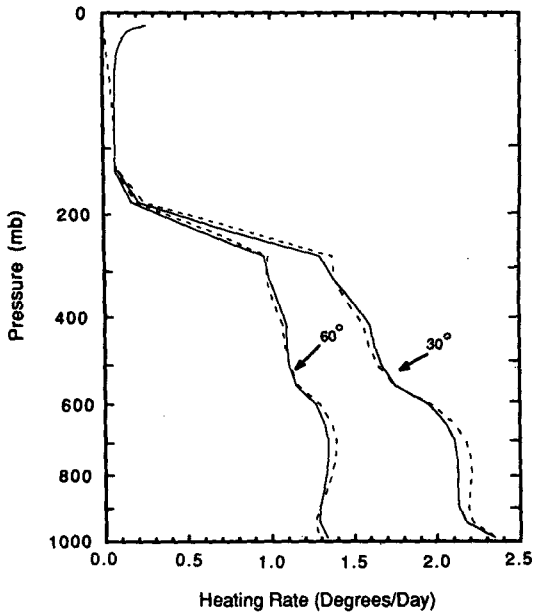

FIG. 5. Heating rate profiles in the near-infrared region for a midlatitude summer atmosphere with a solar zenith angle of 30° and 60°, respectively. Only water vapor is included in the calculations. The solid curves are line-by-line calculations, and the dashed curves are the parameterization using the broadband transmission function of (12). The surface albedo is set to 0.2.

where p/p_r is very small and the absorption is greatly underestimated. However, the ozone heating in this region is very large, as can be seen in Fig. 4. An error of 0.3°C day^{-1} is not significant.

For a scattering atmosphere, the k-distribution method is used for spectral integration of fluxes. Instead of integrating over wavelengths as in (9), the near-infrared flux is computed from

$$F(p) = \int F(p, k) h(k) dk, \quad (14)$$

where $F(p, k)$ is the flux (normalized to μ_0 at $p = 0$) for the absorption coefficient k, $h(k)$ is the flux-weighted k-distribution function defined by

$$h(k) = \sum S_i \Delta\lambda_i h_i(k), \quad (15)$$

where S_i is the mean incoming solar flux in the spectral interval $\Delta\lambda_i$ and h_i is the k-distribution function at p_r and T_r for the interval $\Delta\lambda_i$. In precomputing the function h_i, the spectrum in divided into small intervals, $\Delta\lambda$, such that the variation of solar flux within each interval is small. Details of the derivation of $h_i(k)$ are given in Chou (1986).

In the near-infrared region, the effect of Rayleigh scattering is negligible. For a mixture of water vapor, clouds, and aerosols, the optical thickness, the effective asymmetry factor, and the effective single-scattering albedo are computed from (1a)–(1c). In order to identify the error induced by the scaling approximation

of (11) and, subsequently, by the k-distribution method, two sets of fluxes are computed using the four-stream discrete-ordinate algorithm of Stamnes et al. (1988). In one set of the calculations (labeled LBL+DISORT4 in Tables 5 and 6), the water vapor absorption coefficient is computed at 0.025 cm^{-1} interval using a line-by-line method. In the other set of the calculations (labeled k-Dist+DISORT4 in Table 6), the k-distribution approach is used with the water vapor amount scaled according to (11). The difference between these two sets of calculations is thus entirely caused by the scaling approximation. It can be seen in Table 6 that the scaling approximation of (11) introduces only a 1% error in fluxes.

TABLE 6. The net downward near-infrared fluxes for a midlatitude summer atmosphere computed using different methods. A stratus cloud is set in the layer 800–900 mb. The cloud layer has a scattering optical thickness of 9.7 and an asymmetry factor of 0.843. The Maritime I aerosol model as defined in the ICRCCM is used. The surface albedo is set to 0.2. θ_0 is the solar zenith angle. The units of fluxes are watts per square meter.

Absorption band (cm^{-1})	Top		Surface	
	$\theta_0 = 30°$	$\theta_0 = 60°$	$\theta_0 = 30°$	$\theta_0 = 60°$
2600–4400				
LBL + DISORT4	37.09	20.58	2.60	0.95
LBL + DISORT2	36.49	20.26	2.12	0.70
k-Dist + DISORT4	36.53	20.21	2.74	1.01
Parameterization	36.31	20.00	2.51	0.93
4400–6300				
LBL + DISORT4	67.55	35.35	13.18	5.13
LBL + DISORT2	65.25	34.26	11.25	4.09
k-Dist + DISORT4	67.90	35.44	13.70	5.33
Parameterization	67.06	34.86	12.59	4.95
6300–8200				
LBL + DISORT4	89.86	48.02	17.03	6.76
LBL + DISORT2	87.36	46.78	14.76	5.59
k-Dist + DISORT4	88.46	47.23	17.17	6.83
Parameterization	87.43	46.51	16.10	6.46
8200–9600				
LBL + DISORT4	61.53	30.57	20.64	9.00
LBL + DISORT2	47.21	30.53	19.56	7.15
k-Dist + DISORT4	61.45	31.77	20.68	8.43
Parameterization	60.25	30.99	19.78	8.12
9600–11 600				
LBL + DISORT4	79.93	39.88	39.11	16.23
LBL + DISORT2	75.94	40.31	35.06	12.31
k-Dist + DISORT4	80.31	40.17	38.64	16.08
Parameterization	78.26	39.01	37.14	15.57
11 600–13 100				
LBL + DISORT4	48.32	22.07	39.89	16.97
LBL + DISORT2	44.89	20.35	36.42	15.29
k-Dist + DISORT4	49.60	22.83	39.61	16.85
Parameterization	47.74	21.97	38.08	16.31
13 100–14 500				
LBL + DISORT4	45.59	21.28	34.72	14.69
LBL + DISORT2	42.55	19.73	31.60	13.19
k-Dist + DISORT4	46.55	21.98	33.56	14.20
Parameterization	44.90	21.15	32.37	13.79
Total (2600–14 500)				
LBL + DISORT4	429.87	217.75	167.17	69.73
LBL + DISORT2	409.69	212.22	150.77	58.32
k-Dist + DISORT4	430.80	219.62	166.10	68.73
Parameterization	421.93	214.48	158.67	66.13

Note: DISORT4 and DISORT2 denote four-stream and two-stream discrete-ordinate methods, respectively.

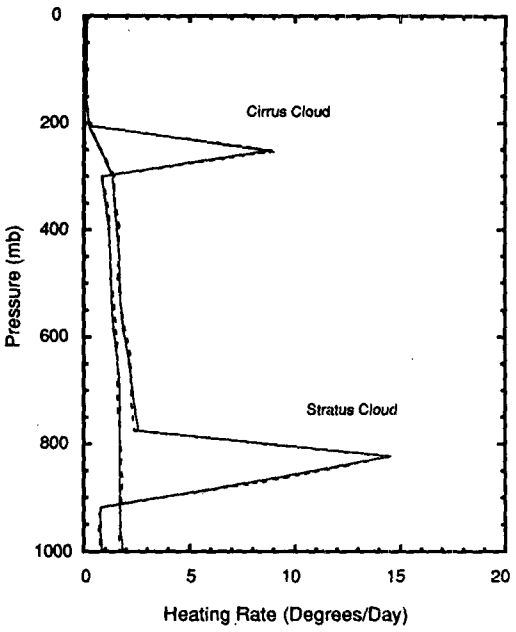

FIG. 6. Heating rate profiles in the near-infrared region for a midlatitude summer atmosphere with a solar zenith angle of 30°. The heating rate profiles are computed separately for a cirrus cloud in 225–275 mb and for a stratus cloud in 800–900 mb. The surface albedo is set to 0.2.

For the parameterization, the k-distribution method is coupled with the two-stream adding method to compute fluxes in the seven absorption bands. A maximum of eight values of k are used for each band, and the corresponding flux-weighted k-distribution function is derived from Table 1 of Chou (1986). Table 5 lists the net downward near-infrared fluxes at the top of the atmosphere and at the surface with the cirrus cloud in the layer 225–275 mb and the stratus cloud in the layer 800–900 mb. Compared to the detailed calculations (LBL+DISORT4), the parameterization underestimates the absorption of near-infrared radiation by the earth–atmosphere system by <2%. On the other hand, the parameterization introduces an error of <5% in the surface flux. The error is primarily caused by the use of the two-stream adding method in computing the cloud reflectance. Figure 6 shows the computed heating rate profiles for the cirrus case and the stratus case. With the use of the cloud single-scattering albedo given in Table 1, the heating in clouds is strong. It reaches 9°C day^{-1} for the cirrus cloud and 15°C day^{-1} for the stratus cloud. The maximum difference between the parameterization and the detailed calculation is

0.5°C day^{-1}, which occurs in the stratus cloud layer. It is noted that cloud optical thickness is often much larger than 9.7, as is used here for the stratus. I have also computed fluxes and heating rate by increasing the cloud optical thickness from 9.7 to 60. Results show that the difference between the fluxes for the detailed calculations and the parameterization is within 4 W m^{-2} at all levels for a solar zenith angle of 30°.

The changes in the atmospheric absorption and in the downward surface fluxes induced by water vapor are shown in Table 4. The results of the parameterization are within 1.5 W m^{-2} of the line-by-line calculations. The median values of the change as derived from the ICRCCM report are shown to be smaller than the line-by-line calculations, indicating a weaker water vapor absorption. Also shown in the table are the effects of the stratus cloud on the atmospheric heating and the surface flux. The difference between the computations of this study and the median values derived from the ICRCCM report is very large (>50 W m^{-2}). This large discrepancy is believed to be caused by the difference in the cloud absorption (or single-scattering albedo) specified in this study and that used by ICRCCM participants. The effects of the stratus cloud on the atmospheric and surface heating shown in the table for parameterization and for the ICRCCM are, therefore, not consistent. Nevertheless, it shows the importance of cloud absorption on the calculation of atmospheric and surface radiation budgets.

7. Computing efficiency

In climate studies a fast and accurate radiation algorithm is needed. However, speed is often gained at the expense of accuracy. In the parameterizations of this study, the reduction in spectral resolution contributes to the largest savings in computing time. In the UV and visible region, the number of spectral intervals is reduced from 127 to 4. In the near-infrared, about a half million sets of line-by-line calculations are reduced to a maximum of eight sets of k-distribution calculations for each absorption band. If cloud and aerosol are treated differently in different absorption bands, then a total of 50 sets of k-distribution calculations are to be carried out. If mean optical properties for the entire near-infrared can be assigned to cloud and aerosol, as is done in atmospheric general circulation models, then it requires only eight sets of k-distribution calculations.

The use of the two-stream adding method to compute fluxes in a scattering atmosphere also reduces significantly the computing time. In this approach, reflectance and transmittance are first computed for each model layer and then for layers combined. A significant portion of the computing time is used to compute the reflectance and transmittance of a scattering layer using the delta-four-stream method. For a nonscattering layer, the reflectance and transmittance are simply given by (2a)–(2c). Thus, the computing efficiency of the two-stream adding method depends on the number of scattering layers involved.

For the case with the stratus cloud in 800–900 mb but without aerosols, there are two scattering layers involved in the calculations. The two-stream adding method is a factor of ~25 faster than the discrete-ordinate algorithm (with four streams) of Stamnes et al. (1988). In the UV and visible region where Rayleigh scattering is involved in all layers, the two-stream adding method is faster than the algorithm of Stamnes et al. (1988) by only a factor of 2–3.

The speed of the parameterization using the two-stream adding method can be further increased by precomputing the transmittance and reflectance instead of calling the delta-four-stream discrete-ordinate algorithm in the calculations. For example, the transmittance and reflectance of each layer due to Rayleigh scattering can be precomputed as a function of the solar zenith angle only. For water clouds, the asymmetry factor can be specified at ~0.845, and the transmittance and reflectance can be precomputed as a function of the optical thickness, the single-scattering albedo, and the solar zenith angle.

When the number of streams is reduced from four to two, the speed of the discrete-ordinate algorithm is enhanced by a factor of 2, but the accuracy is greatly reduced. As shown in Table 6, the use of the two-stream discrete-ordinate algorithm (LBL+DISORT2) introduces an error of 20 W m^{-2} at the top of the atmosphere and 17 W m^{-2} at the surface for the case with a solar zenith angle of 30°. It should be noted that in some atmospheric general circulation models, two-stream approximations are used for computing solar heating. In view of the results shown here, these approximations should be used with extra care.

8. Summary and conclusions

A model for accurate computations of solar radiative transfer in a plane-parallel atmosphere has been developed based on high spectral-resolution calculations of absorption due to ozone and water vapor and detailed calculations of multiple scattering due to clouds, aerosols, and atmospheric gases. The UV and visible region ($\lambda < 0.69$ μm) is grouped into four bands. An effective coefficient for ozone absorption and an effective cross section for Rayleigh scattering are computed for each band. In the near-infrared region ($\lambda > 0.69$ μm), the broadband parameterization is used to compute the absorption by water vapor in a clear atmosphere, and the k-distribution method (with eight values of the absorption coefficient) is applied to each one of the seven water vapor absorption bands in a scattering atmosphere. The reflectance and transmittance of a scattering layer are computed from the algorithm of Liou et al. (1988). The two-stream adding method is then applied to compute fluxes for a composite of

clear and scattering layers. Compared to the high spectral-resolution calculations using the multiple-scattering algorithm of Stamnes et al. (1988), fluxes and heating rate are accurately computed. Errors are generally within a few percent in both the UV and visible region and the near-infrared region.

The Rayleigh scattering and the ozone absorption of solar radiation are found to be equally important in affecting surface radiation. By grouping the UV and visible region into four bands, the Rayleigh scattering and the ozone absorption of solar radiation can be accurately computed in the ultraviolet region and the photosynthetically active radiation (PAR) region. The solar radiation routine developed in this study can be applied not only for climate studies but also for studies on the photolysis in the upper atmosphere and the photosynthesis in the biosphere.

The absorption of solar radiation due to oxygen and carbon dioxide has been parameterized by Chou (1990) and is not addressed in this study. The computer program we have developed for the solar flux calculation does include the absorption by both oxygen and carbon dioxide.

The high accuracy of flux and heating rate calculations is achieved with a reasonable amount of computing time. With the atmosphere divided into 42 layers and a stratus cloud in the 800–900-mb layer, the speed for computing flux and heating profiles in the solar spectral region is a factor of 5–10 faster than that in the thermal infrared region using the algorithm of Chou et al. (1991).

Acknowledgments. The author is grateful to Dr. Si-Chee Tsay of the University Space Research Association for inspiring discussions and for providing the FORTRAN program for the discrete-ordinate radiative transfer algorithm. The author is also grateful to Dr. Qiang Fu of the University of Utah for providing the FORTRAN program for the delta four-stream radiative transfer algorithm. This work was supported by the NASA Radiation Processes Program managed by Dr. Timothy Suttles.

REFERENCES

Chou, M.-D., 1986: Atmospheric solar heating rate in the water vapor bands. *J. Climate Appl. Meteor.*, **25,** 1532–1542.

——, 1990: Parameterizations for the absorption of solar radiation by O_2 and CO_2 with application to climate studies. *J. Climate,* **3,** 209–217.

——, and A. Arking, 1981: An efficient method for computing the absorption of solar radiation by water vapor. *J. Atmos. Sci.,* **38,** 798–807.

——, and L. Kouvaris, 1986: Monochromatic calculations of atmospheric radiative transfer due to molecular line absorption. *J. Geophys. Res.,* **91,** 4047–4055.

——, D. P. Kratz, and W. Ridgway, 1991: Infrared radiation parameterizations in numerical climate models. *J. Climate,* **4,** 424–437.

Coakley, J. A., Jr., R. D. Cess, and Franz B. Yurevich, 1983: The effect of tropospheric aerosols on the earth's radiation budget: A parameterization for climate models. *J. Atmos. Sci.,* **40,** 116–138.

Ellingson, R. G., and Y. Fouquart, 1990: Radiation and climate: Intercomparison of Radiation Codes in Climate Models (ICRCCM), World Climate Research Programme-39, 38 pp.

Kiehl, J. T., and T. Yamanouchi, 1985: A parameterization for absorption due to the A, B, and γ oxygen bands. *Tellus,* **37B,** 1–6.

——, C. Bruehl, and T. Yamanouchi, 1985: A parameterization for absorption due to the near infrared bands of CO_2. *Tellus,* **37B,** 189–196.

King, M. D., L. F. Radke, and P. V. Hobbs, 1990: Determination of the spectral absorption of solar radiation by marine stratocumulus clouds from airborne measurements within clouds. *J. Atmos. Sci.,* **47,** 894–907.

Lacis, A. A., and J. E. Hansen, 1974: A parameterization for the absorption of solar radiation in the earth's atmosphere. *J. Atmos. Sci.,* **31,** 118–133.

Liou, K.-N., Q. Fu, and T. P. Ackerman, 1988: A simple formulation of the delta-four-stream approximation for radiative transfer parameterizations. *J. Atmos. Sci.,* **45,** 1940–1947.

McClatchey, R. A., R. W. Fenn, J. E. A. Selby, F. E. Volz, and J. S. Garing, 1972: Optical properties of the atmosphere, 3rd ed. AFCRL-72-0497, 108 pp. [NTIS N7318412]

Rothman, L. S., R. R. Gamache, A. Barbe, A. Goldman, J. R. Gillis, L. R. Brown, R. A. Toth, J.-M. Flaud, and C. Camy-Peyret, 1983: AFGL atmospheric line parameters compilation: 1982 edition. *Appl. Opt.,* **22,** 2247–2256.

Stamnes, K., and S.-C. Tsay, 1990: Optimum spectral resolution for computing atmospheric heating and photodissociation rates. *Planet. Space Sci.,* **38,** 807–820.

——, ——, W. Wiscombe, and K. Jayaweera, 1988: Numerically stable algorithm for discrete-ordinate-method radiative transfer in multiple scattering and emitting layered media. *Appl. Optics,* **27,** 2502–2509.

Stephens, G., and S.-C. Tsay, 1990: On the cloud absorption anomaly. *Quart. J. Roy. Meteor. Soc.,* **116,** 671–704.

Tsay, S.-C., K. Stamnes, and K. Jayaweera, 1989: Radiative energy budget in the cloudy and hazy arctic. *J. Atmos. Sci.,* **46,** 1002–1018.

World Meteorological Organization, 1985: *Atmospheric Ozone, Global Ozone Research and Monitoring Project,* Vol. I, Report No. 16, 392 pp.